

Quantum Hall effect in narrow graphene ribbons

H. Hettmansperger,¹ F. Duerr,² J.B. Oostinga,² C. Gould,² B. Trauzettel,¹ and L.W. Molenkamp²

¹*Institut für Theoretische Physik und Astrophysik, University of Würzburg, Am Hubland, 97074 Würzburg, Germany*

²*Physikalisches Institut (EP3), University of Würzburg, Am Hubland, 97074 Würzburg, Germany*

(Dated: September 11, 2018)

The edge states in the integer quantum Hall effect are known to be significantly affected by electrostatic interactions leading to the formation of compressible and incompressible strips at the boundaries of Hall bars. We show here, in a combined experimental and theoretical analysis, that this does not hold for the quantum Hall effect in narrow graphene ribbons. In our graphene Hall bar, which is only 60 nm wide, we observe the quantum Hall effect up to Landau level index $k = 2$ and show within a zero free-parameter model that the spatial extent of the compressible and incompressible strips is of a similar magnitude as the magnetic length. We conclude that in narrow graphene ribbons the single-particle picture is a more appropriate description of the quantum Hall effect and that electrostatic effects are of minor importance.

PACS numbers: 73.63.-b, 81.05.ue, 73.43.-f

I. INTRODUCTION

The discovery of graphene is intimately related to the first measurements of the integer quantum Hall effect in this material system.^{1,2} It was observed as early as 2005 that the integer quantum Hall effect shows an anomalous sequence of Hall plateaus in the Hall conductivity $\sigma_{xy} = 4(k + 1/2) e^2/h$ due to the graphene-specific Berry phase that finds its origin in the bipartiteness of the honeycomb lattice. This is a crucial difference from quantum Hall effect measurements in more established material systems such as two-dimensional electron gases (2DEGs) in semiconductor heterostructures.

A second distinction between the quantum Hall effect in graphene and that in ordinary 2DEGs is suggested by two terminal conductance studies on narrow ribbons,^{3,4} where conductance quantization was interpreted in quantum Hall terms, even though the ribbons are narrower than the typical separation between edge states in a 2DEG. To confirm the validity of this interpretation, we have fabricated a 60-nm-wide graphene Hall bar, allowing for proper four terminal measurement of R_{xy} and confirming that quantum Hall edge states do survive even in such narrow devices in graphene.

In order to reconcile these observations with the conventional picture of edge-state separation, we need to recall the physics of edge states in ordinary 2DEGs. The first detailed description of edge-state transport in the quantum Hall regime was provided by Halperin⁵ using a noninteracting electron picture. While this model is useful in describing much of the relevant physics, it was subsequently found that such a picture does not in general properly account for the position of the edge states. A more exact description emerges when considering the influence of electrostatic interactions between the electrons that form the quantum Hall state and the surrounding electrons in the substrate and the nearby metallic gates. In ordinary 2DEGs, it is well established that these electrostatic interactions lead to the formation of compressible and incompressible strips.^{6,7} Indeed, the effect of electrostatic interactions is of such importance that, in many cases, the single-particle picture fails to provide even a qualitative description of experiment. The situation is different in narrow graphene structures, where, as our zero-free-parameter model shows,

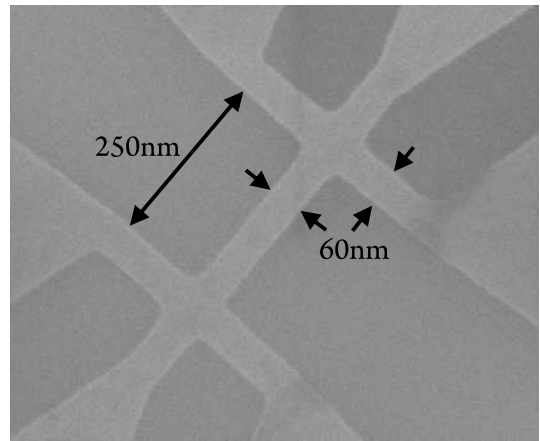


FIG. 1. (Color online) SEM image of a plasma patterned six-terminal graphene Hall bar with $w = 60$ nm and $l = 250$ nm.

the relevant length scale for the single-particle picture — the magnetic length $l_B = \sqrt{\hbar/eB}$ — is similar to the width of the compressible and incompressible strips.

II. EXPERIMENTAL PART

A scanning electron micrograph (SEM) of our sample is shown in Fig. 1. It is made from single-layer graphene flakes exfoliated from an HOPG block onto a highly p-doped Si substrate having a 285 nm thick SiO_2 cap layer. After contacting Ti/Au electrodes, these flakes are etched in an Ar/ O_2 plasma to obtain narrow Hall bars with six terminals. To reduce residual contaminations, the etched structure is annealed at 200 °C in forming gas for about 2 h. The sample is studied at the base temperature of a dilution refrigerator using standard low-noise ac measurement techniques.

Preliminary characterization of the sample is done at 4.2 K, where, as typical for ribbons of width below 100 nm, the conductance G of the sample is strongly suppressed in the vicinity of the charge neutrality point, which is at $V_g^D \approx 7.5$ V. At high electron and hole concentrations, the field-effect mobility of

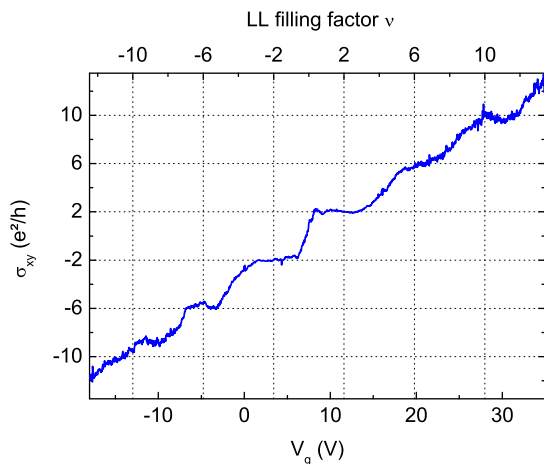


FIG. 2. (Color online) Hall conductivity σ_{xy} as a function of gate voltage V_g and Landau level filling factor $\nu = h/(e^2 B)C_g(V_g - V_g^D)$ at $B = 11$ T and 30 mK. (Figure adapted from Ref. 9.)

the charge carriers is $\mu = \frac{l}{2a_r C_g} \frac{dC_g}{dV_g} \approx 1500 \text{ cm}^2/\text{Vs}$, where the effective gate capacitance $C_g \approx 210 \text{ } \mu\text{F}/\text{m}^2$ is determined from Hall measurements at various gate voltages V_g . This corresponds to a diffusion constant of $D \simeq 0.01 \text{ m}^2/\text{s}$ and a mean free path of $l_m \simeq 20 \text{ nm}$. Such small values are typical for plasma-etched graphene nanoribbon devices and are a consequence of the great amount of edge disorder in these systems.⁸

We recently observed the quantum Hall effect in very narrow graphene wires.⁹ A representative example of such a measurement is shown in Fig. 2, where we plot the measured Hall conductivity σ_{xy} as a function of the back-gate voltage V_g and filling factor $\nu = \pm 4(k + 1/2)$ at $B = 11$ T. The occurrence of conductance plateaus at $k = 0, 1,$ and 2 is typical for Dirac fermions and clearly confirms that our sample is mono layer graphene. In general, σ_{xy} plateaus are well developed if the energy spacing between the corresponding Landau levels is much larger than their broadening Γ . In graphene the former, given by Eq. (7), decreases with increasing filling (i.e., the index k), whereas the broadening $\Gamma = \hbar v_F/l_m \simeq 30 \text{ meV}$ is constant. This explains why only the $k = 0, 1,$ and 2 plateaus are visible up to $B = 11$ T, with the $k = 0$ plateaus being most pronounced. We found this observation remarkable in view of previous experience with (Al,Ga)As-based structures. Therefore, we decided to investigate the electrostatics of the edge channels in more detail, which is presented in the next sections.

III. THEORETICAL PART

From a theoretical point of view, the essence of our device is an etched graphene ribbon separated from a metallic back gate by an insulating SiO_2 layer. We note that the thickness, of the gate insulator is a significant parameter because, for very thin thicknesses tunneling becomes as important as electrostatic effects. Our geometry is therefore fundamentally differ-

ent from the one used in recent STM studies of the spacial extent of edge channels in graphene resting directly on graphite, where the thickness of the gate insulator is basically 0 (i.e., the distance between the graphene and the graphite substrate).¹⁰

We now examine the consequences of our geometry on the accepted models by Chklovskii, Shklovskii, and Glazman (CSG)⁶ as well as Chklovskii, Matveev, and Shklovskii (CMS).⁷ In the electrostatic theories of CSG and CMS, a 2DEG is laterally confined by electric fields originating from gate electrodes which are in plane with the 2DEG. In the absence of magnetic fields, the electrostatic solution of such a two-dimensional problem was provided by Larkin and Shikin.¹¹ They find a charge density distribution which reduces from its bulk value to 0 at the boundary of the electron gas. Although the confinement of mobile electrons in these models is generated by gates, the authors of Refs. 6 and 7 argue that their results also apply to etched structures of conventional heterostructures. This is justified by surface states which lead to Fermi level pinning and negative charges accumulate at the edges. Inner electrons are repelled, yielding the same depletion effect as split gates. However, as shown by Silvestrov and Efetov (SE),¹² the situation is substantially different in the case of a graphene nanoribbon. Since the edges of this two-dimensional material end abruptly, they act as hard instead of soft-wall boundaries. Assuming a constant electrostatic potential in a ribbon positioned in the xz plane, such that in the transverse x direction no electric force acts on its excess electrons, SE derived an expression for the charge density. If the ribbon width $2a_r$ is smaller than the gate dielectric thickness b , the electron density across the ribbon is, to a good approximation, given by¹²

$$\rho(x, y) = \frac{\sigma}{\pi} \frac{\delta(y)}{\sqrt{a_r^2 - x^2}} \left\{ 1 - C_2 \left(\frac{a_r}{b} \right)^2 \left(\frac{2x^2}{a_r^2} - 1 \right) \right\}, \quad (1)$$

where $C_2 \equiv \sum_{n=1}^{\infty} \frac{\epsilon}{1-\epsilon} \left(\frac{1-\epsilon}{1+\epsilon} \right)^n \frac{1}{4n^2}$ is a numerical constant¹³ that, for a dielectric constant $\epsilon \simeq 3.9$ as in the case of SiO_2 , has a value of 0.175. The charge per unit length σ is linearly related to the back-gate potential V_g ,¹²

$$V_g = \frac{4\sigma}{\epsilon + 1} \left\{ \ln \frac{4b}{a_r} + C_0 + \left(\frac{a_r}{b} \right)^2 C_2 \right\}, \quad (2)$$

with $C_0 \equiv \sum_{n=2}^{\infty} \frac{2\epsilon}{1-\epsilon} \left(\frac{1-\epsilon}{1+\epsilon} \right)^n \ln n$.

The inverse-square-root edge singularity in Eq. (1) is in stark contrast to the soft density profiles ($\rho \sim \sqrt{x}$) predicted at the edges of conventional heterostructures.^{6,7,11} In the following, we analyze the impact of this diverging density distribution on the formation of compressible and incompressible strips in graphene.

The formulas above are valid for any metallic strip with a hard-wall boundary. The graphene-specific physics comes into play with quantum effects. Evidently, the Pauli principle prevents the excess electrons from all being in the same state. When the Fermi wavelength varies slowly on the considered length scale (here the width of the ribbon), one can divide the system into many elements of sizes where equilibrium thermodynamics is still applicable. By using this Thomas-Fermi

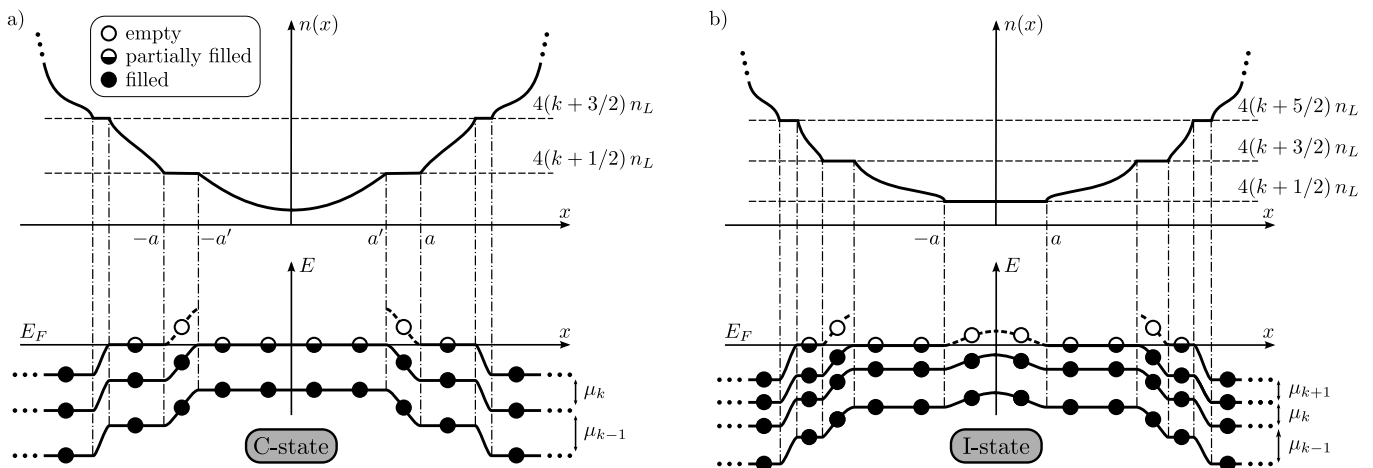


FIG. 3. (Color online) Schematic of the compressible and incompressible strips in graphene, showing the electron density $\propto n(x)$ and the Landau levels with their local fillings. In (a) the ribbon is in a C state with a compressible strip at its center whereas in (b) it is in an I state with an incompressible strip in the middle. The regions near the edges of the ribbon where the Landau levels increase very sharply due to hard-wall confinement are not shown. In these regions of size $\sim l_B$ away from the edges, the electrostatic analysis is no longer applicable.¹⁴

approximation, SE defined a local Fermi momentum for each element and derived a relation between the inhomogeneous charge density given by Eq. (1) and the potential felt by an individual electron. At zero temperature and in the limit of rather narrow ribbons ($a_r \ll b$), the curly bracket in Eq. (1) reduces to 1, and the potential has the form

$$U(x) = -\hbar v_F \sqrt{\sigma/e} \left(\frac{1}{a_r^2 - x^2} \right)^{1/4}, \quad (3)$$

with v_F the Fermi velocity in graphene. The derived expression is valid at distances $\delta x \gtrsim a_r^{1/3} \left(\frac{e}{\sigma} \right)^{2/3}$ from the strip edges, where the Thomas-Fermi approximation is applicable. This potential should be viewed as a quantum correction to the electrostatic potential and describes locally the energy difference between the constant Fermi energy and the Dirac point.

Knowing the electron distribution and the potential in a graphene ribbon, we can now adapt the CMS formalism to graphene. Making use of the semiclassical electrostatic picture described above, we expect, for a finite magnetic field, the scenario sketched in Fig. 3. As in the case of the 2DEG in Ref. 7, the electron density $\sim n(x)$ in our graphene ribbon is divided into alternating compressible and incompressible strips. The latter are characterized by filled Landau levels and describe local unscreened regions in which electrons have no possibility to reorder. This is due to the large energy gap they must overcome in order to find unoccupied states in one of the nearby empty levels. On the other hand, compressible strips are characterized by partially filled Landau levels residing at the Fermi level. The many unoccupied states allow for the electrons to rearrange and minimize their energy such that the electric field is locally screened. In general, two situations are possible. In Fig. 3(a), we show a C state that describes a central compressible strip in the k -th Landau level which is partially filled near $x = 0$. Upon decreasing the magnetic field strength or increasing the density of excess charges, the

k -th Landau level gets filled and the ribbon is driven into an I state with an incompressible strip at the center [cf. Fig. 3(b)].

IV. RESULTS

The basic formalism used in Ref. 7 to determine the widths and positions of the compressible and incompressible strips in a gate confined 2DEG is also valid in graphene nanoribbons. Imposing the same requirements on the electrostatic boundary conditions as within the framework of the CMS model, and solving for our geometry leads to the following set of equations:

$$[\nu(0) - 4(k + 1/2)] n_L + n''(0) \frac{a^2 + a'^2}{4} = 0, \quad (4)$$

$$-\frac{2\pi e n''(0) a}{3(\epsilon + 1)} \left\{ (a^2 + a'^2) E \left[\sqrt{1 - (a'/a)^2} \right] - 2(a')^2 K \left[\sqrt{1 - (a'/a)^2} \right] \right\} = -\mu_k, \quad (5)$$

TABLE I. Experimental parameters used in the modeling.

Quantity	Value
Magnetic field B	11 T
Insulator dielectric constant ϵ	3.9, SiO ₂
Thickness of insulator b	0.3 μm
Half-width of graphene ribbon a_r	30 nm
Back-gate potential V_g	-20 to 35 V

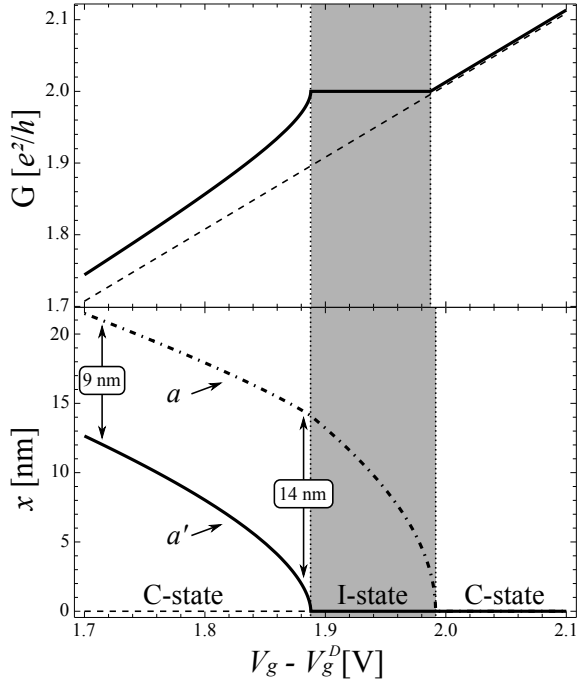


FIG. 4. (Color online) Top: Two-terminal conductance plateau corresponding to Landau level index $k = 0$, plotted over the back-gate voltage V_g . The charge neutrality point is at V_g^D , and the dashed line indicates G_0 . Bottom: The position and width of the compressible and incompressible strips are plotted, which, in Fig. 3, correspond to the occupation level $4(k + 1/2)n_L$ with $k = 0$. The dashed-dotted line shows a , the outer edge position; the solid line shows a' , the inner edge position of the incompressible strips. In the upper graph the suppressed contribution of distant incompressible strips to the conductance at the I-C transition is incorporated, whereas in the lower graph it is neglected, resulting in a slight mismatch in width of the shaded areas.

$$\begin{aligned} \nu(0) - \nu_B(0) &= -\frac{n''(0)(a - a')^2}{4n_L} \\ &= \frac{(a - a')^2}{a^2 + a'^2} [\nu(0) - 4(k + 1/2)]. \end{aligned} \quad (6)$$

Here, E and K are elliptic integrals, and the quantities a and a' determine the positions and widths of the compressible and incompressible strips next to $x = 0$. The energy difference,

$$\mu_k \equiv \frac{\hbar v_F}{l_B} \left(\sqrt{2(k+1)} - \sqrt{2k} \right), \quad (7)$$

is that of adjacent Landau levels (see Fig. 3) and depends on the index k , the Fermi velocity v_F , and the magnetic length $l_B = \sqrt{\hbar/eB}$. The occupation number of these levels is defined by $\nu_B(0) \equiv n_B(x=0)/n_L$, with $n_B(0)$ the electron concentration at magnetic field strength B in the center of the ribbon, and $n_L \equiv 1/2\pi l_B^2$ the Landau level degeneracy. Furthermore, we define $\nu(0) \equiv n(x=0)/n_L$, with $n(x)$ the electron concentration in the absence of a magnetic field, which can be extracted from $\rho(x, y) = e n(x) \delta(y)$ via Eq. (1).

Taken together, Eqs. (4), (5), and (6) represent a complete system from which the quantities a , a' , and $\nu_B(0)$ can be derived. The latter is linearly related to the two-terminal conductance⁷ via

$$G = \frac{e^2}{h} \nu_B(0). \quad (8)$$

In order to analyze the results provided by this model, we use the experimental parameters listed in Table I, and solve for a , a' , and ν_B . Since Eqs. (4), (5), and (6) are derived under the assumption that $n(x) \simeq n(0) + \frac{1}{2}n''(0)x^2$, we are limited to a parameter range where this approximation is valid. This is ensured when a and a' are small compared to a_r , which is the case at the transition from a C to an I state caused by increasing the doping or decreasing the magnetic field. In the upper graph in Fig. 4, we show the conductance plateau which corresponds to the Landau level with index $k = 0$. From the electrostatic point of view, incompressible strips next to $x = 0$, characterized by local regions with an additional charge accumulation, are described by dipolar strips.⁶ Although the calculated charge density distribution, Eq. (1), is not altered on a rough scale at any reasonable magnetic field, the formation of such strips leads to a small enhancement in charge concentration at $x = 0$. Thus, it is reasonable that the conductance, given by Eq. (8), lies above the dashed line, which indicates $G_0 \equiv \frac{e^2}{h} \nu(0)$. From the lower graph in Fig. 4, we can read off the positions and widths of the compressible and incompressible strips which correspond to the occupation level $4(k + 1/2)n_L$ with $k = 0$. In the C state, before the formation of the conductance plateau, the incompressible strips next to the central compressible one have a width of ~ 9 nm ... 14 nm. This, however, contradicts a crucial assumption of the electrostatic model,⁷

$$l_B \sqrt{k} \ll (a - a'). \quad (9)$$

For the quasi classical electrostatic treatment above to be justified, the size of the electron wave function determined by the magnetic length should be much smaller than the length scales provided by the widths of the compressible and incompressible strips. Since $l_{B=11T} \sim 8$ nm, our experiment is in the crossover regime to the conventional single-particle picture of ballistic transport.¹⁵ The latter is mandatory at high quantum numbers k where condition (9) is strongly violated. For the first several plateaus, however, the electrostatic model which results in Eqs. (4), (5), and (6) is still relevant, as Eq. (9) is approximately valid. Also note that the widths of incompressible strips located at x_k scale as $\sim 1/\sqrt{n'(x_k)}$.⁶ Thus, for narrow ribbons with large $n'(x_k)$ and therefore small $a - a'$, condition (9) is violated much earlier as for wide ribbons with expanded incompressible strips. Furthermore, since $n'(x_k)$ increases as we approach the edges, the spatial extent of the edge states within the electrostatic picture is much narrower in our graphene ribbon compared to l_B . Hence, we show that the CSM picture of transport in the quantum Hall regime breaks down here and the simpler single-particle picture not only suffices but, indeed, is essential to correctly describe the physics.

V. COMPARISON OF THEORY AND EXPERIMENT

Comparing the data on the $k = 0$ plateau, corresponding to filling factor $\nu = 2$ in Fig. 2, with the theoretical result given in Fig. 4, we find discrepancies in width and location, both measured in units of the back-gate voltage. Our electrostatic model leads to very narrow plateaus occurring at gate voltages which are too small by a factor of ~ 3 to 4. This disagreement is consistent with theory overestimating the gate capacitance, which is a commonly observed discrepancy in graphene nanoribbons.¹⁶ The narrowness of the theoretically derived plateaus compared to their experimental widths can be explained by disorder, which is certainly present in the device, but neglected in our model. As realized in Refs. 6 and 7, disorder leads to localization in a compressible liquid a low small enough density, such that at the I to C state transition there is a range of voltage where Landau levels which locally (in the vicinity of $x = 0$) start to fill up cannot contribute to the conductance.

VI. CONCLUSIONS

We have performed four terminal transport measurements on a 60-nm-wide Hall bar of graphene. Our results validate the interpretation that the Hall effect is responsible for the quantized conductance in narrow ribbons. A quantitative study of the electrostatics of graphene nanoribbons, and its implication for the spatial extent of edge states in such devices, confirms that, indeed, the formation of compressible and incompressible strips which dominate the physics of traditional 2DEG devices is of minor importance here. Instead, the single-particle picture is more appropriate.

ACKNOWLEDGMENTS

B.T. would like to thank Misha Fogler for interesting discussions at the KITP in Santa Barbara. This work was supported by the DFG in the framework of the strategic Japanese-German cooperative program and the European Science Foundation (ESF) under the EUROCORES Program EuroGRAPHENE.

-
- ¹ K. S. Novoselov, A. K. Geim, S. V. Morozov, D. Jiang, M. I. Katsnelson, I. V. Grigorieva, S. V. Dubonos, and A. A. Firsov, *Nature* **438**, 197 (2005).
- ² Y. Zhang, Y.-W. Tan, H. L. Stormer, and P. Kim, *Nature* **438**, 201 (2005).
- ³ R. Ribeiro, J.-M. Poumirol, A. Cresti, W. Escoffier, M. Goiran, J.-M. Broto, S. Roche, and B. Raquet, *Phys. Rev. Lett.* **107**, 086601 (2011).
- ⁴ S. Schmidmeier, S. H. Jhang, J. Wurm, Y. Skourski, J. Wosnitza, C. Strunk, D. Weiss, K. Richter, and J. Eroms, *Phys. Rev. B* **85**, 195432 (2012).
- ⁵ B. I. Halperin, *Phys. Rev. B* **25**, 2185 (1982).
- ⁶ D. Chklovskii, B. Shklovskii, and L. Glazman, *Phys. Rev. B* **46**, 4026 (1992).
- ⁷ D. Chklovskii, K. Matveev, and B. Shklovskii, *Phys. Rev. B* **47**, 12605 (1993).
- ⁸ F. Molitor, J. Guttiner, C. Stampfer, S. Droscher, A. Jacobsen, T. Ihn, and K. Ensslin, *Journal of Phys.: Cond. Mat.* **23**, 243201 (2011).
- ⁹ F. Duerr, J.B. Oostinga, C. Gould, and L.W. Molenkamp, *Phys. Rev. B* **86**, 081410(R) (2012).
- ¹⁰ G. Li, A. Luican, D. Abanin, L. Levitov, and E.Y. Andrei, arXiv:1203.5540.
- ¹¹ I. Larkin and V. Shikin, *Phys. Lett. A* **151**, 335 (1990).
- ¹² P. Silvestrov and K. Efetov, *Phys. Rev. B* **77**, 155436 (2008).
- ¹³ The equation for C_2 in Ref. 12 has a typo. A factor 1/4 is missing.
- ¹⁴ We note here that the full density profile, which includes both the bulk and the edge behavior, may even lead to the formation of counter-propagating edge channels as discussed by A. Shylau, I. Zozoulenko, H. Xu, and T. Heinzl, *Phys. Rev. B* **82**, 121410 (2010).
- ¹⁵ M. Büttiker, *Phys. Rev. B* **41**, 7906 (1990).
- ¹⁶ C. Lian, K. Tahy, T. Fang, G. Li, H.G. Xing, and D. Jena, *Appl. Phys. Lett.* **96** 103109 (2010).